New Journal of Physics
The open access journal for physics

Neutrino mass sensitivity by MAC-E-Filter based time-of-flight spectroscopy with the example of KATRIN

Nicholas Steinbrink[1,3], **Volker Hannen**[1], **Eric L Martin**[2], **R G Hamish Robertson**[2], **Michael Zacher**[1] **and Christian Weinheimer**[1]

[1] Institut für Kernphysik, Westfälische Wilhelms-Universität Münster, Wilhelm Klemm-Strasse 9, D-48149 Münster, Germany
[2] Center for Experimental Nuclear Physics and Astrophysics, and Department of Physics, University of Washington, Seattle, WA, USA
E-mail: n.steinbrink@uni-muenster.de

New Journal of Physics **15** (2013) 113020 (29pp)
Received 6 August 2013
Published 11 November 2013
Online at http://www.njp.org/
doi:10.1088/1367-2630/15/11/113020

Abstract. The KArlsruhe TRItium Neutrino (KATRIN) experiment aims at a measurement of the neutrino mass with a 90% confidence limit (CL) sensitivity of 0.2 eV/c^2 by measuring the endpoint region of the tritium β decay spectrum from a windowless gaseous molecular tritium source using an integrating spectrometer of the magnetic adiabatic collimation with an electrostatic filter (MAC-E-Filter) type. We discuss the idea of using the MAC-E-Filter in a time-of-flight mode (MAC-E-TOF) in which the neutrino mass is determined by a measurement of the electron TOF spectrum that depends on the neutrino mass. MAC-E-TOF spectroscopy here is a very sensitive method since the β-electrons are slowed down to distinguishable velocities by the MAC-E-Filter. Their velocity depends strongly on their surplus energy above the electric retarding potential. Using MAC-E-TOF, a statistical sensitivity gain is expected. Because a small number of retarding-potential settings is sufficient for a complete

[3] Author to whom any correspondence should be addressed.

measurement, in contrast to about 40 different retarding potentials used in the standard MAC-E-Filter mode, there is a gain in measurement time and hence statistical power. The improvement of the statistical uncertainty of the squared neutrino mass has been determined by Monte Carlo simulation to be a factor 5 for an ideal case neglecting background and timing uncertainty. Additionally, two scenarios to determine the TOF of the β-electrons are discussed, which use the KATRIN detector for creating the stop signal and different methods for obtaining a start signal. These comprise the hypothetical case of an 'electron tagger' which detects passing electrons with minimal interference and the more realistic case of 'gated filtering', where the electron flux is periodically cut off by pulsing the pre-spectrometer potential.

Contents

1. Introduction

Since the neutrino oscillation results from the Super Kamiokande Experiment in 1998 it is evident that neutrinos have a non-zero rest mass contradictory to the standard model. In a number of experiments on solar, atmospheric, reactor and accelerator neutrinos, the mass differences between the three neutrino mass eigenstates and the three mixing angles have been

measured. However, these experiments are not sensitive to the absolute scale of the neutrino mass which needs to be determined in an independent experiment [1–5].

A precise knowledge of the neutrino mass is not only important due to its role in cosmological structure formation [6] but also to find out which mass generation mechanism is responsible for the neutrino sector. An important experimental distinction to be made is the determination of the mass hierarchy, i.e. whether the mass states are normally ordered ($m_1 < m_2 < m_3$), inverted ($m_3 < m_1 < m_2$) or quasi-degenerate ($m_1 \approx m_2 \approx m_3$). A determination of the mass hierarchy allows to confirm or rule out models of ν-mass generation. For instance, certain see-saw models, which introduce new physics in the Higgs sector, favour a quasi-degenerate scenario [7]. Moreover, most models introduce additional heavy neutrino mass states, usually identical to or strongly mixed with right-handed ('sterile') flavour states. If one of these additional mass states, however, is sufficiently light (i.e. in the eV to keV range) and at least slightly mixed with the 'active' flavour states ν_e, ν_μ, ν_τ, the sterile neutrino becomes observable in neutrino oscillation experiments and in β spectra.

Hints towards the existence of light sterile neutrinos in the eV range currently arise for instance from the reactor neutrino anomaly [8], the calibration of solar neutrino experiments Gallex and SAGE [9–12] and the short baseline accelerator neutrino oscillation experiments LSND [13] and MiniBooNE [14]. That there might be more than three active neutrinos is also compatible with the total radiation content of the universe obtained from big bang nuclei synthesis and the investigation of the cosmic microwave background [6, 15, 16]. Sterile neutrinos in the keV range, however, are predicted by the warm dark matter (WDM) scenario, which is supported by several astrophysical observations, e.g. the too little structure at galactic scales ('missing satellite problem') [17]. We will discuss briefly at the end that the method of time-of-flight (TOF) spectroscopy with gated filter proposed in this paper is not only interesting for the search of sub-eV and eV neutrino masses in β spectra but also for keV neutrinos.

In probing the absolute ν mass scale, the KArlsruhe TRItium Neutrino (*KATRIN*) experiment [18] is designed to measure the neutrino mass, which, in the quasi-degenerate regime accessible to KATRIN, is an incoherent sum of the light mass eigenstates weighted with their mixing to the electron neutrino [19]

$$m_{\nu_e} = \sqrt{\sum_i |U_{ei}^2|\, m_i^2}. \tag{1}$$

This observable will be determined with a sensitivity of $<0.2\,\mathrm{eV}/c^2$ (90% CL). The predecessor experiments in Mainz [20] and Troitsk [21] were successful in finding a 95% CL upper limit of $m_{\nu_e} \leqslant 2.3\,\mathrm{eV}/c^2$ and $m_{\nu_e} \leqslant 2.05\,\mathrm{eV}/c^2$, respectively. A further improvement of the sensitivity beyond the KATRIN design goal would be interesting since the KATRIN sensitivity limit lies in the critical transition region between hierarchical and the quasi-degenerate scenarios and the other methods sensitive to the neutrino mass, the search for neutrino-less double β-decay [22] and cosmology [6] are of similar sensitivity.

KATRIN measures the endpoint region of the β^- decay spectrum of tritium, which is a function of m_{ν_e}. Neglecting the recoil energy of the nucleus as well as radiative corrections the

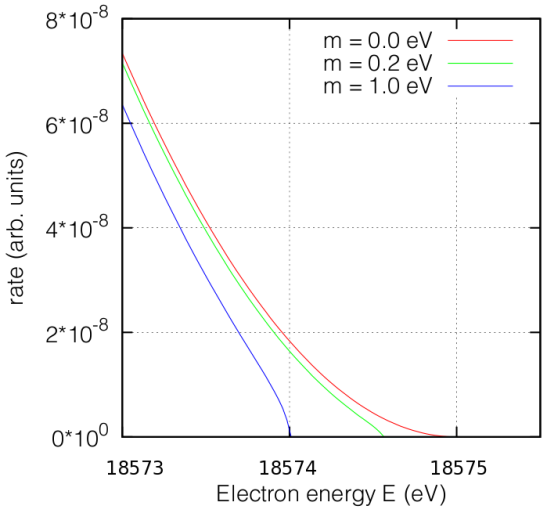

Figure 1. Effects of the neutrino mass on the last part of the beta spectrum. The molecular final state spectrum has been omitted for simplicity.

differential decay rate [19, 23] is at first order given by

$$\frac{\mathrm{d}R}{\mathrm{d}E}(E) = N\frac{G_\mathrm{F}^2}{2\pi^3\hbar^7c^5}\cos^2(\theta_\mathrm{C})|M|^2\ F(E,Z')p(E+m_\mathrm{e}c^2) \times \sum_i P_i(E_0-V_i-E)\sqrt{(E_0-V_i-E)^2-m_{\nu_\mathrm{e}}^2c^4}, \tag{2}$$

where E is the kinetic electron energy, θ_C the Cabbibo angle, N the number of tritium atoms, G_F the Fermi constant, M the nuclear matrix element, $F(E,Z')$ the Fermi function with the charge of the daughter ion Z', p the electron momentum, P_i the probability to decay to an excited electronic and rotational–vibrational state with excitation energy V_i [24–26] and E_0 the beta endpoint, i.e. the maximum kinetic energy in case of $m_{\nu_\mathrm{e}} = 0$. A non-vanishing neutrino mass changes the spectrum in such a way that the maximal kinetic energy of the decay electrons is lowered to $E_\mathrm{max} = E_0 - m_{\nu_\mathrm{e}}c^2$ and that in the vicinity of the endpoint $E_0 \approx 18.575\,\mathrm{keV}$ the phase space density of the electron is reduced. Figure 1 shows the endpoint region for different neutrino mass values m_{ν_e}.

KATRIN uses a large spectrometer of magnetic adiabatic collimation with an electrostatic filter (MAC-E-Filter) type and a windowless gaseous molecular tritium source for the measurement of m_{ν_e} [18]. The sensitivity of KATRIN is principally constrained by the diameter of its spectrometer and its tritium source, which influence the energy resolution and the signal rate, respectively. Since KATRIN reaches the technical limits regarding these parameters, extending the sensitivity would require complementary methods.

In this paper, the idea of a new measurement principle is presented. It can be performed at a suitable MAC-E-Filter setup like the main spectrometer of KATRIN. Instead of the classic integrating mode, where the count rate is scanned as a function of the retarding potential, the TOF of every electron passing through the spectrometer is measured. Since the endpoint region of the decay spectrum of tritium is a function of m_{ν_e}, the distribution of flight times depends as well on the neutrino mass. The MAC-E-Filter TOF mode (MAC-E-TOF) is expected to improve the sensitivity on m_{ν_e}. Since for each retarding potential not only a count rate but a full TOF

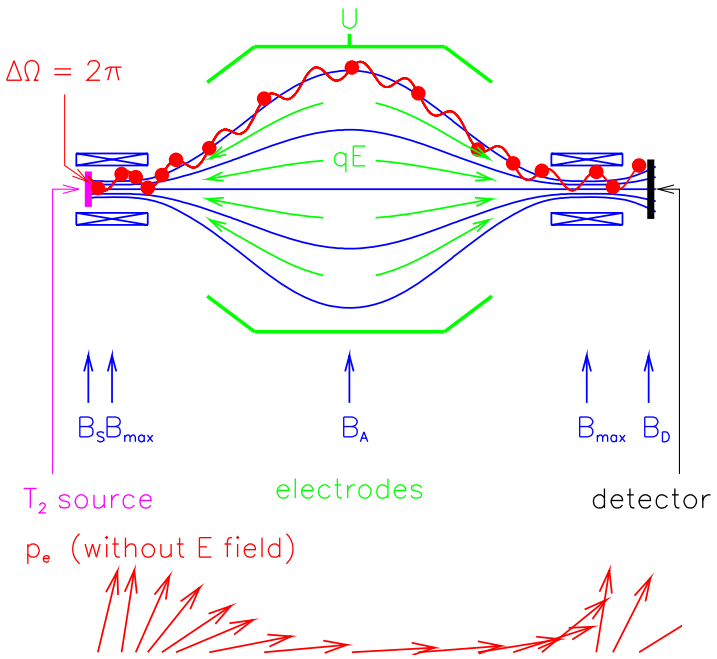

Figure 2. Principle of the MAC-E-Filter [18]. The transverse momentum is transformed adiabatically into longitudinal momentum. The electron energy is then analysed by an electrostatic retarding potential.

spectrum is measured, the number of potential steps can be reduced without sensitivity loss. The measurement time which is gained that way can be invested in obtaining more statistics.

2. Classic magnetic adiabatic collimation with an electrostatic filter technique

In a classic tritium neutrino experiment the beta spectrum (2) is scanned with a high pass filter using different threshold energies qU. Thereby, the principle of MAC-E-Filter [27] is applied. To achieve a sharp energy resolution, the electron motion which is isotropic at the source is converted into a longitudinal movement in the analysing plane where the retarding potential qU is applied. The transformation is performed by applying high magnetic fields B_S at the source and B_D at the detector, and a low field B_{min} in the analysing plane. Under adiabatic conditions the magnetic moment μ times the relativistic factor γ is conserved,

$$\gamma\mu = \frac{p_\perp^2}{B} = \text{const}, \tag{3}$$

meaning that the momentum component transverse to the B field lines $p_\perp$ is converted into parallel momentum in low magnetic field regions (figure 2). This parallel beam of electrons is energetically analysed by applying the retarding voltage U. The relative sharpness of this energy high-pass filter depends only on the ratio of the minimum magnetic field B_{min} reached at the electrostatic barrier in the so called analysing plane and the maximum magnetic field B_{max} between β-electron source and spectrometer, where E is the starting energy of the electron from an isotropically emitting source:

$$\frac{\Delta E}{E} = \frac{B_{min}}{B_{max}}. \tag{4}$$

It is beneficial to place the electron source in a magnetic field B_S somewhat lower than B_{max}. Thus the magnetic-mirror effect based on the adiabatic invariant (3) prevents electrons with large starting angles at the source, and therefore long flight paths inside the source, from entering the MAC-E-Filter. Only electrons having starting angles θ_S at B_S of

$$\sin^2(\theta_S) \leqslant \frac{B_S}{B_{max}} \tag{5}$$

are able to pass the pinch field B_{max}.

The transmission probability $T(E, U)$ of the MAC-E-Filter for an isotropic emitting electron source of energy E can be analytically calculated. Normalized to unity at full transmission it reads

$$T(E,U) = \begin{cases} 0 & \text{for } E \leqslant qU, \\ \dfrac{1-\sqrt{1-\frac{E-qU}{E}\cdot\frac{B_S}{B_{min}}}}{1-\sqrt{1-\frac{B_S}{B_{max}}}} & \text{for } qU < E < qU + \Delta E, \\ 1 & \text{for } E \geqslant qU + \Delta E. \end{cases} \tag{6}$$

In the neutrino mass experiment the count rate is then measured at the detector for each retarding potential qU which is related to (2) by

$$R_T(qU) = \frac{\Delta\Omega}{4\pi}\left(\int_{qU}^{E_0 - m_{\nu_e}c^2} \frac{dR}{dE}(E)\, T'(E, qU)\, dE\right) + b, \tag{7}$$

where b is the background rate, $\frac{\Delta\Omega}{4\pi}$ the accepted solid angle with $\frac{\Delta\Omega}{4\pi} = (1 - \cos\theta_{max})/2$ and T' the response function of the experiment (figure 3). The latter is the convolution of the transmission function T (6) with a function describing the inelastic energy losses [28].

3. MAC-E time-of-flight (TOF) spectroscopy

3.1. General idea

An alternative idea is to use *MAC-E-Filter time of flight (MAC-E-TOF) spectroscopy* to measure the neutrino mass. The TOF of a β decay electron through a MAC-E-Filter like the main spectrometer of KATRIN is a function of the kinetic energy and the emission angle. The distribution of the kinetic energies is in first order governed by the beta spectrum (2) which contains the neutrino mass. By measuring the TOF distribution (TOF spectrum) of the electrons, one can reconstruct the parameters determining the beta spectrum, including $m^2_{\nu_e}$. Such a method would feature mainly two intrinsic advantages.

On the one hand the MAC-E-Filter slows down the electrons near the retarding energy. While the relative velocity differences between raw beta decay electrons near the endpoint are tiny, a TOF measurement of beta electrons passing through a MAC-E-Filter will be very sensitive to subtle energy differences just above the retarding energy. It can be seen (figure 4) that in principle electron energy differences even below the resolution of the MAC-E-Filter, which is $\Delta E = 0.93$ eV for 18.5 keV electrons in case of KATRIN, can be resolved, given a sufficient time resolution.

On the other hand, the standard MAC-E mode measures only the count rate for each retarding energy, as described above. In contrast, the TOF spectroscopy mode measures the

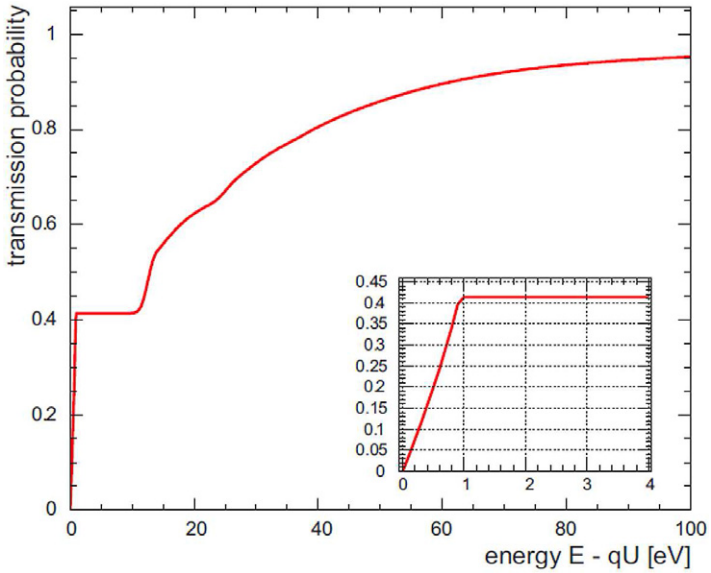

Figure 3. Response function of the KATRIN experiment for isotropically emitted electrons [18]. The function is given as a convolution of the transmission function T (6) with a function describing the inelastic energy losses in the source [18]. The inset shows the rise of the response functions at small surplus energies $E - qU$ governed by the fraction of electrons of approximately 41% that have undergone no inelastic scattering process. Therefore this rise corresponds to the shape of the transmission function T.

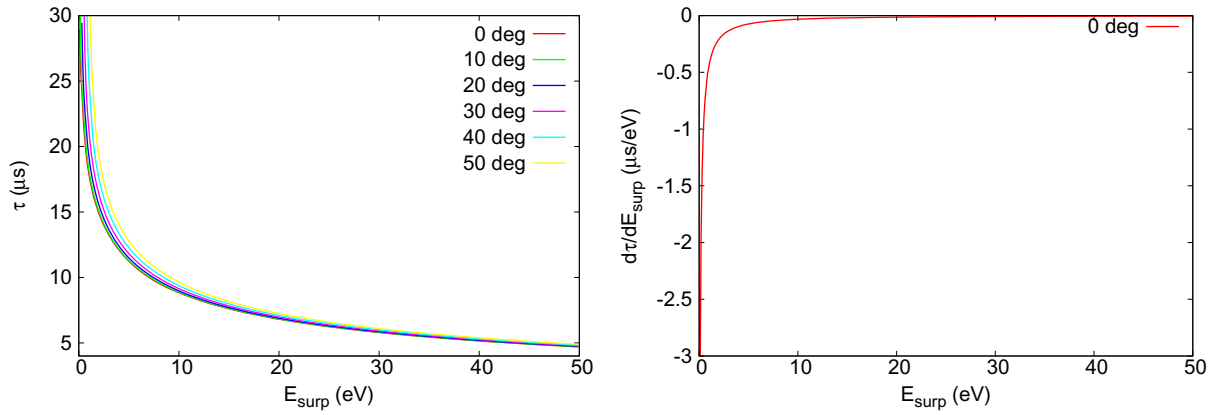

Figure 4. TOF for different starting angles (top) and first derivative for $\theta = 0^\circ$ (bottom) as a function of the surplus energy $E_{\mathrm{surp}} = E - qU$ for a central detector pixel. The starting angle is limited to 50.77° due to the KATRIN field design. The first derivative reflects the sensitivity on energy differences and is especially large close to the retarding energy qU.

TOF for each decay electron. Thus a full TOF spectrum, sensitive to $m^2_{\nu_e}$, is obtained for each retarding energy. For suitable measurement conditions, this gain of information improves the statistics.

The combination of these advantages allows useful optimizations. In principle it would be sufficient to measure only at a single retarding energy near the beta endpoint, though a small number of selected retarding energies might be more sensitive. Since the systematic uncertainty on $m^2_{\nu_e}$ grows as the retarding energy is decreased, the goal is to minimize the amount of measurements far from the beta endpoint. The TOF method could in principle provide this and concentrate the measurement on a few retarding energies near the endpoint, each of them delivering a full TOF spectrum from which $m^2_{\nu_e}$ can be disentangled.

3.2. Mathematical model

The aim is to state the TOF spectrum as a function of certain fit parameters. These comprise the beta endpoint E_0 and the square of the neutrino mass $m^2_{\nu_e}$, as well as the relative signal amplitude S which depends on several factors. Thereby, E_0 is in principle known from the ^{3}He–T mass difference measurements in penning traps to 1.2 eV precision [29]. However, this is not precise enough to fix it *ab initio*. Improvements on the beta endpoint precision are on the way [30]. For a full study also a constant background rate b needs to be fitted, which is however dependent on the implementation of the measurement method. In order to obtain an expression for the TOF spectrum, the TOF has to be known as a function of the kinetic energy E and the starting angle θ first and then has to be weighted by the corresponding distributions given by the windowless gaseous tritium source [31].

3.2.1. TOF as function of E and θ. Within the main spectrometer the principle of adiabatic motion, where the magnetic moment is constant (3), is valid to good approximation. Using a simplified geometry, we take only the field on the z-axis into account and neglect magnetron drifts. The B field then is only a function of the z coordinate. Then, the transverse momentum of an electron can be derived from equation (3) as a function of z,

$$p^2_\perp(z) = p(z_{\text{source}})^2 \sin^2\theta(z_{\text{source}}) \frac{B(z)}{B(z_{\text{source}})}, \tag{8}$$

where $p(z_{\text{source}})$, $\theta(z_{\text{source}})$ and $B(z_{\text{source}})$ are the electron momentum, its emission angle and the total magnetic field at the electron's starting position z_{source}. The fraction reflects the role of the adiabatic magnetic field geometry of the MAC-E-filter: as the field $B(z)$ decreases, the transverse momentum is converted continuously into longitudinal momentum. The relativistic energy of the electron is given by the energy–momentum-relation

$$E^2_{\text{rel}}(z) = p^2_\parallel(z)c^2 + p^2_\perp(z)c^2 + m^2_e c^4. \tag{9}$$

Since the total energy $E_{\text{tot}} = E_{\text{rel}} + E_{\text{pot}} = E_{\text{kin}} + m_e c^2 + E_{\text{pot}}$ is conserved, we can express the relativistic energy as a function of z:

$$\begin{aligned} E_{\text{rel}}(z) &= E_{\text{rel}}(z_{\text{source}}) - E_{\text{pot}}(z) + E_{\text{pot}}(z_{\text{source}}) \\ &= E_{\text{kin}}(z_{\text{source}}) + m_e c^2 - q\,\Delta U(z), \end{aligned} \tag{10}$$

where $\Delta U(z)$ is the difference of the retarding voltage at the source and at z,

$$\Delta U(z) = |U(z) - U(z_{\text{source}})|, \tag{11}$$

and q is the magnitude of the electron charge. Combining equations (8)–(10), we derive an expression for the longitudinal momentum as a function of z only in terms of the field B and

the potential difference ΔU:

$$p_{\parallel}^2(z)c^2 = \left(E^2 + 2E\, m_e c^2\right)\left(1 - \sin^2\theta \frac{B(z)}{B(z_{\text{source}})}\right) + q^2\Delta U^2(z) - 2q\,\Delta U(z)\left(E + m_e c^2\right) \tag{12}$$

with the abbreviations $E := E_{\text{kin}}(z_{\text{source}})$ and $\theta := \theta(z_{\text{source}})$. The TOF is determined by integrating the reciprocal parallel velocity $1/v_{\parallel} = \gamma m/p_{\parallel} = E_{\text{rel}}/p_{\parallel}c^2$ over the measurement path:

$$\tau(E,\theta) = \int \mathrm{d}z\, \frac{1}{v_{\parallel}} = \int_{z_{\text{start}}}^{z_{\text{stop}}} \mathrm{d}z\, \frac{E + m_e c^2 - q\,\Delta U(z)}{\sqrt{p_{\parallel}^2(z)c^2}\, c}. \tag{13}$$

The lower bound z_{start} of the integration interval depends on where the start signal time is measured[4] while z_{stop} corresponds to the z-position of the detector. As the adiabatic approximation (3) is valid through the whole transport section, this position is arbitrary. The starting angle $\theta = \theta(z_{\text{source}})$ is automatically transformed to its correct value at the start position $\theta(z_{\text{start}})$ by (12) because only the ratio of local and source magnetic field $B(z)/B(z_{\text{source}})$ matters but not the field changes between $B(z_{\text{source}})$ and $B(z_{\text{start}})$.

The integral (13) is only correct for electrons emitted in the centre of the fluxtube $r = 0$ since the integration path is identical with the z-axis. As shown in figure 2, the electrons perform a cyclotron motion around the B field lines, where for the flight-times only the velocity component parallel to the B field lines $v_{\parallel}$ needs to be considered. Electrons emitted at $r = 0$ take a path different from the z-axis. This is, however, not a real shortcoming of our method because at KATRIN the starting position can be reconstructed by the point of arrival on the multipixel detector. Therefore we do not expect significant changes in sensitivity depending on the electron emission radius. For this in-principle study of the statistical sensitivity we consider it to be sufficient to use the central electron tracks only.

3.3. TOF spectrum

Equation (13) presumes a fixed kinetic starting energy and starting angle as arguments. For a real source, these parameters are not fixed but follow physical distributions. In order to be calculated numerically, the differential TOF spectrum $\frac{\mathrm{d}N}{\mathrm{d}t}$ is discretized into bins of constant length Δt and integrated over each bin j, leading to a binned spectrum

$$F(t_j) := \int_{t_j}^{t_{j+1}=t_j+\Delta t} \mathrm{d}t\, \frac{\mathrm{d}N}{\mathrm{d}t}. \tag{14}$$

The number of events in a certain TOF bin depends on the distribution of starting energies and angles E and θ,

$$\begin{aligned} F(t_j) &= \iint_{(E,\theta)\ \text{with}\ t_j \leqslant \tau(E,\theta) \leqslant t_{j+1}} \frac{\mathrm{d}^2N}{\mathrm{d}\theta\,\mathrm{d}E}\,\mathrm{d}\theta\,\mathrm{d}E \\ &= \int_0^{\theta_{\max}} \int_{E_j(\theta)}^{E_{j+1}(\theta)} \frac{\mathrm{d}^2N}{\mathrm{d}\theta\,\mathrm{d}E}\,\mathrm{d}\theta\,\mathrm{d}E, \end{aligned} \tag{15}$$

[4] This should preferably be at the beginning of the MAC-E-Filter, in case of KATRIN at the entrance of the main spectrometer.

where $\frac{\mathrm{d}^2N}{\mathrm{d}\theta\,\mathrm{d}E}$ is the double differential event rate as function of E and θ. The integral limits $E_j(\theta)$ and $E_{j+1}(\theta)$ are defined in such way that $\tau(E_j,\theta) = t_j$ and $\tau(E_{j+1},\theta) = t_{j+1}$, respectively. At first order, $\frac{\mathrm{d}^2N}{\mathrm{d}\theta\,\mathrm{d}E}$ is given by the double differential decay rate $\frac{\mathrm{d}^2R}{\mathrm{d}\theta\,\mathrm{d}E}$ into the accepted solid angle $\frac{\Delta\Omega}{4\pi}$,

$$\frac{\mathrm{d}^2N}{\mathrm{d}\theta\,\mathrm{d}E} \approx \frac{\mathrm{d}^2R}{\mathrm{d}\theta\,\mathrm{d}E}. \tag{16}$$

As the double differential is proportional to the joint probability distribution of emitting an electron with energy E at a polar angle of θ and, furthermore, the angle and the energy are uncorrelated in case of a non-oriented radioactive source, the quantity can be separated into a product of the single differential decay rate $\frac{\mathrm{d}R}{\mathrm{d}E}$, as given by (2), and the angular probability distribution $g(\theta)$ [32],

$$\frac{\mathrm{d}^2R}{\mathrm{d}\theta\,\mathrm{d}E} = \frac{\mathrm{d}R}{\mathrm{d}E}\,g(\theta). \tag{17}$$

In case of an isotropic tritium source, a sine law applies for the angular distribution

$$g(\theta) = \tfrac{1}{2}\sin\theta. \tag{18}$$

This angular distribution function is normalized to unity over the full solid angle 4π. Since for KATRIN the polar angle is restricted to $\theta_{\max} = 50.77^\circ$, the signal rate is implicitly reduced by a factor

$$\int_0^{\theta_{\max}} \mathrm{d}\theta\; g(\theta) = \frac{\Delta\Omega}{4\pi} = \frac{(1-\cos\theta_{\max})}{2}, \tag{19}$$

which is enforced by the upper integral bound $\theta_{\max}$ in (15).

The approximation (16) is only valid in case of an ideal tritium source. However, quite a few electrons lose energy in elastic and inelastic scattering processes with the tritium molecules. These losses are dependent on the emission angle since the path through the tritium source increases with $1/\cos\theta$. Thus, for the differential rate of events which are actually analysed in the main spectrometer, given by $\frac{\mathrm{d}^2N}{\mathrm{d}\theta\,\mathrm{d}E}$ in (15), starting energies and angles become correlated. Additionally, the signal rate decreases due to several losses inside the experiment. A factor $\epsilon_{\mathrm{flux}} \approx 0.83$ applies since the flux tube transported through the whole system corresponds to a diameter of 82 mm w.r.t. the beam tube diameter of 90 mm, meaning that only a part of the windowless gaseous tritium source (WGTS) tube is imaged onto the detector. Furthermore, the detector efficiency gives an additional factor of $\epsilon_{\mathrm{det}} \approx 0.9$.

In total, the true event rate can be calculated by applying the correction factors and convoluting the beta spectrum with an energy loss function, which gives

$$\begin{aligned}\frac{\mathrm{d}^2N}{\mathrm{d}\theta\,\mathrm{d}E} &= \epsilon_{\mathrm{flux}}\,\epsilon_{\mathrm{det}}\,g(\theta)\,\frac{\mathrm{d}R}{\mathrm{d}E} \otimes f_{\mathrm{loss},\theta} \\ &= \epsilon_{\mathrm{flux}}\,\epsilon_{\mathrm{det}}\,g(\theta)\left(p_0(\theta)\,\frac{\mathrm{d}R}{\mathrm{d}E} + \sum_{n=1}^{\infty} p_n(\theta)\,\frac{\mathrm{d}R}{\mathrm{d}E} \otimes f_n\right),\end{aligned} \tag{20}$$

where the f_n is the energy loss function of scattering order n which is defined recursively through the single scattering energy loss function f_1 as

$$f_n = f_{n-1} \otimes f_1 \quad (n > 1). \tag{21}$$

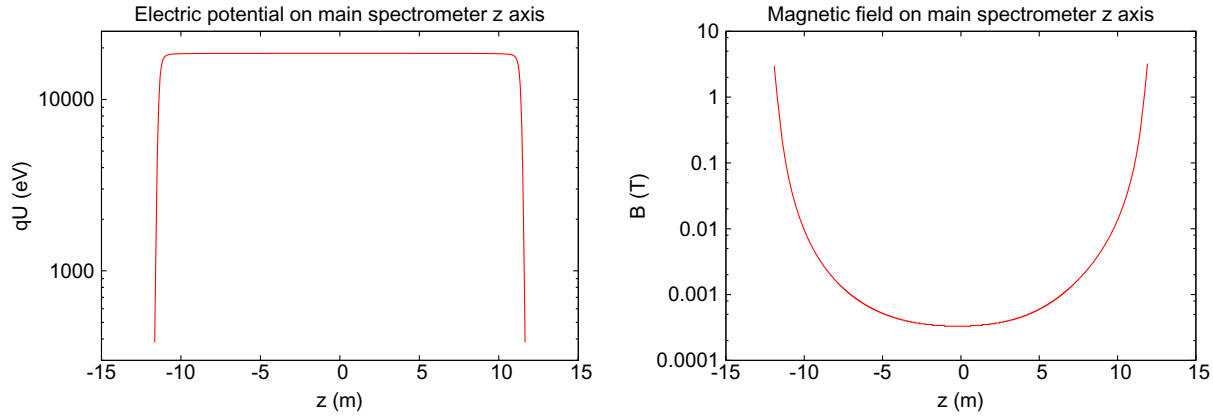

Figure 5. Electric potential (a) and magnetic field (b) along the inner axis of the KATRIN main spectrometer generated by simulation. The scaling of the electric potential depends on the retarding energy qU.

The function $f_1(\Delta E)$ is the probability density of losing the energy ΔE in a singular scattering event [28]. The functions of f_n can then correspondingly be interpreted as the same for n-fold scattering. In this equation, all changes of the angle of the electron during scattering are neglected. p_n is the probability that an electron is scattered n times. If we again neglect changes of the angle, it is a function of the emission angle θ and given by a Poisson law

$$p_n(\theta) = \frac{\lambda^n(\theta)}{n!} \mathrm{e}^{-\lambda^n(\theta)} \,. \tag{22}$$

Here, the expectation value λ is given in terms of the column density ρd, the mean free column density ρd_{free} and the scattering cross section σ_{scat} as

$$\lambda(\theta) = \int_0^1 \mathrm{d}x \, \frac{\rho d \, x}{\rho d_{\mathrm{free}} \cos\theta} = \int_0^1 \mathrm{d}x \, \frac{\rho d \, x \sigma_{\mathrm{scat}}}{\cos\theta} \,, \tag{23}$$

where the integration factor x accounts for the fact that the starting position of the electron inside the WGTS is statistically distributed.

4. Simulation of principle

4.1. Study of TOF spectra

To calculate the TOF spectrum according to (15) the input parameters have to be obtained. A model for the one-dimensional field maps $\Delta U(z)$ and $B(z)$ in (13) has been determined by the KATRIN simulation tools *magfield* and *elcd3_2* [33] using a modestly simplified geometry that contains the most important coils and electrodes in the main spectrometer (figure 5). A model for the energy loss function (21) has been determined in the past by electron scattering experiments on hydrogen [28] and refined by using excitation and ionization data from hydrogen molecules [34]. The final-state excitation spectrum of the daughter molecules has been used from [24].

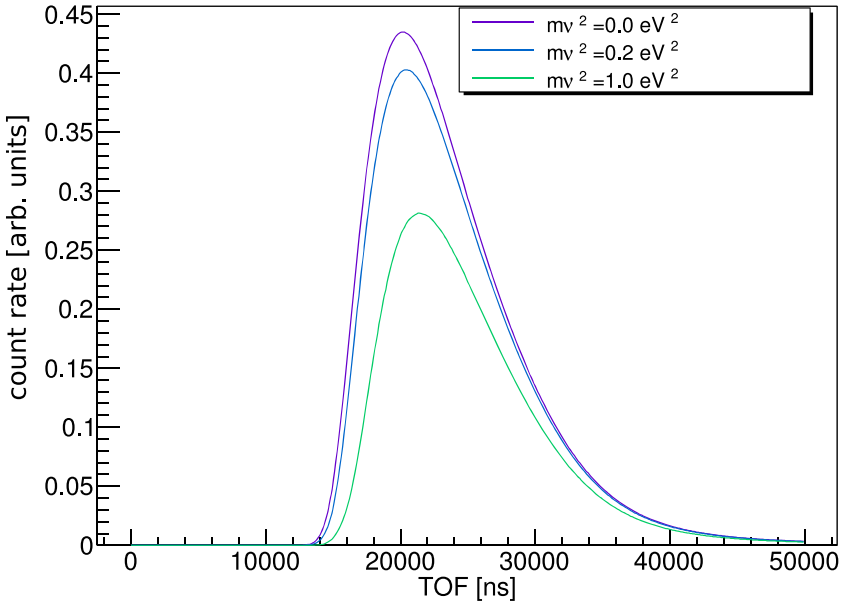

Figure 6. Effects on the TOF spectrum for different neutrino masses at a high retarding potential (18 570 eV) with endpoint $E_0 = 18\,574.0$ eV. The scaling of the y-axis is arbitrary.

A typical set of simulated TOF spectra for different neutrino mass squares is shown in figure 6. The following details and parameter-dependent behaviour can be observed:

- For each spectrum, there exists a minimal TOF $t_{\min}$. This corresponds to the maximum kinetic emission energy that an electron can have, given by $E_{\max} = E_0 - m_{\nu_e}c^2$.
- From $t_{\min}$ on, a steep slope begins, leading soon to a maximum somewhat above $t_{\min}$, followed again by a long, slow fall. The maximum can be explained by the fact that the higher the energy becomes, the lower the number of electrons is, due to the shape of the end of the beta spectrum, whereas the 'TOF energy density', i.e. the interval size of the energy that corresponds to a certain TOF bin, increases. These effects balance each other, leading to a maximum somewhere in the middle.
- There is no maximal TOF. The closer the energy of an electron is to the retarding energy, the slower it will be. That means that electrons with an energy infinitesimally above the retarding energy will have an infinite TOF.
- If the neutrino mass square $m^2_{\nu_e}$ is changed, the main signature is a change in count-rate and a change of the shape especially at the short-time end of the spectrum (figure 6).
- A higher retarding energy qU leads to a clearer distinction between spectra for different neutrino masses. The reason is that the neutrino mass is mainly visible in the last few eV of the beta spectrum. Therefore, it seems optimal for the TOF mode to measure with retarding energies near the endpoint. However, due to the lower count rate and the difficult decorrelation of neutrino mass square and endpoint, measurements from lower retarding energies should be added to the data.

4.2. Neutrino mass fits

4.2.1. Method. In order to study the statistical uncertainty we used the spectra to fit Monte Carlo (MC) data. The MC data have been obtained by creating Poisson distributed random numbers based on the predictions from (15), where certain choices of the parameters $m^2_{\nu_e}$ and E_0 as well as the retarding energy qU and the measurement time have been assumed. The data are fitted in this self-consistent method by the models (15) using a χ^2 minimization method. If multiple measurements with different qU are assumed, they can be fitted with a common chi square function by adding the chi square functions from each run. If the fit is performed correctly, the chosen parameters $m^2_{\nu_e}$ and E_0 are reproduced. Additionally, estimates for the parameter errors can be determined as

$$\chi^2(\phi_0 \pm \Delta\phi_\pm) = \chi^2(\phi_0) + 1, \tag{24}$$

where ϕ_0 is a parameter estimate and $\Delta\phi_\pm$ are the requested, not necessarily symmetric parameter error bars [32]. To obtain a symmetric χ^2 parabola for neutrino masses near zero, there must also be an extension for a negative $m^2_{\nu_e}$ that joins smoothly with the physical spectrum for $m^2_{\nu_e} > 0$. To accomplish this, to each term in the sum of the beta spectrum (2) a factor

$$f_i = \left(1 + \frac{m_{\mathrm{eff}}}{\epsilon_i} \mathrm{e}^{-(1+\epsilon_i/m_{\mathrm{eff}})}\right) \tag{25}$$

is applied in case of $m^2_{\nu_e} < 0$ and $\epsilon_i + m_{\mathrm{eff}} > 0$. In this expression, the abbreviations $\epsilon_i = E_0 - V_i - E$ and $m_{\mathrm{eff}} = \sqrt{-m^2_{\nu_e}}$ have been used [35]. This method allows a simple but realistic prediction of the statistical uncertainty of $m^2_{\nu_e}$.

4.2.2. Results. In order to determine the improvement potential by the TOF mode, an optimal choice of the measurement times of the runs with different retarding energies qU has to be made. For KATRIN a total on-line time of 3 years is planned, which has to be distributed among the retarding energies. We used a simple algorithm where we discretized the retarding potentials and the measurement time and determined the statistical uncertainty with the method above for all possible permutations. The results are shown in table 1. At the MC data creation, a neutrino mass of zero has been assumed. In this case, the average of the fit uncertainties $m^2_{\nu_e}$, as given by (24), describes the sensitivity on the neutrino mass squared.

The comparison shows that it is in principle sufficient to measure at only one retarding energy. If this single retarding energy is close to the endpoint, the correlation between the parameters E_0 and $m^2_{\nu_e}$ becomes weaker at the cost of losing count-rate. It turns out that it is beneficial to combine measurements at more than one retarding energy, where this relation between lowest retarding energy and correlation coefficient does not necessarily hold true (see table 1). In almost all tested cases using multiple retarding potentials a solid decorrelation without suffering from too little count-rate has been possible.

The results in table 1 correspond to the optimum case since background, time uncertainty and other limitations have been neglected. They reflect the maximal improvement potential that can be achieved with a TOF mode. The motivation to neglect the background in the optimum case is based on the idea that a sensitive TOF measurement method may be able to reduce the background, too, depending on the implementation of the measurement. It can be shown that, compared with the statistical sensitivity for the reference configuration of KATRIN, $\sigma_{\mathrm{stat}}(m^2_{\nu_e}) = 0.018\,\mathrm{eV}^2/c^4$, an improvement of up to a factor ~5–6 by TOF spectroscopy is

Table 1. Average statistical uncertainty $\langle\sigma_{\mathrm{stat}}(m^2_{\nu_e})\rangle = \langle\frac{1}{2}(|\Delta m^2_{\nu_e -}| + |\Delta m^2_{\nu_e +}|)\rangle$ (arithmetic mean of positive and negative error of ten simulations and fits), average fit parameters $\langle\bar{E}_0\rangle$ and $\langle\bar{m}^2_{\nu_e}\rangle$, as well as Pearson's correlation coefficient $R(E_0, m^2_{\nu_e})$ of uniform and optimized distributions and the KATRIN standard mode. The total assumed measurement time is the KATRIN standard of 3 years [18], distributed among four retarding energies $qU = 18\,550$, $18\,555$, $18\,560$ and $18\,565$ V as well as for single retarding potentials for $m^2_{\nu_e} = 0\,\mathrm{eV}^2/c^2$, $E_0 = 18\,575$ eV and $b = 0$. The choice of retarding potentials for the TOF mode is motivated by the idea that a choice of a few potentials close to the endpoint will likely improve the systematics additionally to the statistical uncertainty.

Fraction of measurement time per retarding energy	Distribution type	Lowest retarding energy (eV)	Mean stat. error $\langle\sigma_{\mathrm{stat}}(m^2_{\nu_e})\rangle$ (eV^2/c^4)	Mean fitted endpoint $\langle\bar{E}_0\rangle$ (eV)	Mean fitted ν mass squared $\langle\bar{m}^2_{\nu_e}\rangle$ (eV^2/c^4)	Mean correlation coefficient $R(E_0,m^2_{\nu_e})$
$(\frac{3}{12}, \frac{3}{12}, \frac{3}{12}, \frac{3}{12})$	Uniform	18 550	0.0033	18 574.9997	0.0004	0.65
$(\frac{1}{12}, \frac{0}{12}, \frac{3}{12}, \frac{8}{12})$	Optimized	18 550	0.0032	18 575.0002	0.0013	0.70
$(0, \frac{4}{12}, \frac{4}{12}, \frac{4}{12})$	Uniform	18 555	0.0034	18 575.0002	0.0015	0.73
$(0, \frac{2}{12}, \frac{1}{12}, \frac{9}{12})$	Optimized	18 555	0.0034	18 575.0002	0.0006	0.72
$(0, 0, \frac{6}{12}, \frac{6}{12})$	Uniform	18 560	0.0036	18 575.0002	0.0014	0.74
$(0, 0, \frac{4}{12}, \frac{8}{12})$	Optimized	18 560	0.0035	18 575.0007	0.0034	0.76
(1, 0, 0, 0)	Single	18 550	0.0035	18 575.0000	0.0004	0.82
(0, 1, 0, 0)	Single	18 555	0.0036	18 575.0000	0.0003	0.88
(0, 0, 1, 0)	Single	18 560	0.0038	18 574.9999	−0.0015	0.79
(0, 0, 0, 1)	Single	18 565	0.0039	18 574.9998	0.0007	0.66
–	Standard mode	18 555	0.020			
–	Standard mode	18 550	0.019			
–	Standard mode	18 545	0.018			

possible. The actual improvement factor, however, depends on the method by which the TOF determination is implemented.

Furthermore, one can conclude that even a reduction of the systematic uncertainty might be possible with the TOF mode. This is due to the fact that the systematic uncertainty at KATRIN depends heavily on the measurement interval at which the spectrum is scanned [18]. That is mainly caused by the uncertainty of the parameters of the electron energy loss which becomes more important at lower retarding energies. An ideal TOF mode, in contrast, would allow one to measure solely at higher retarding energies.

For further analyses, the optimal distribution for the case of 18 560 eV lowest retarding energy has been taken which is likely a good compromise between statistical and systematic uncertainty. An example for a fit, based on this measurement time distribution, is shown in figure 7.

5. Principles of electron tagging

The creation of a TOF spectrum requires a start and a stop time associated with the passage of each detected electron through the spectrometer. The stop time is easily derived from the

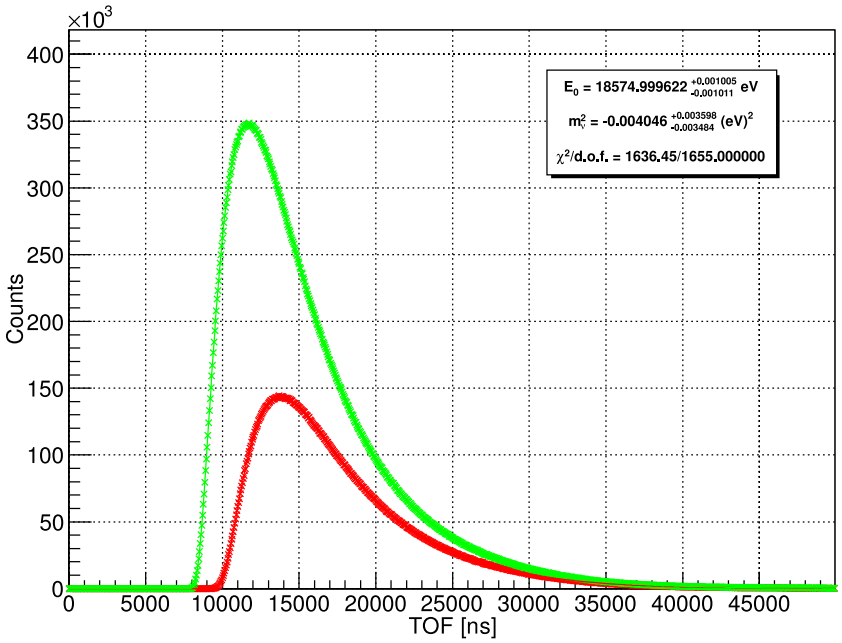

Figure 7. Example of simulated data and fit of a TOF spectrum for the optimal case of no background and no time uncertainty. For the fit, a measurement time of 3 years was assigned 2/3 to 18 565 eV (red points online, smaller amplitude) and 1/3 to 18 560 eV (green points online, larger amplitude). These correspond to the optimum distribution for lowest retarding energy of 18 560 eV in table 1.

pulse produced when the electron is absorbed in the focal-plane detector. A start time must be produced by some device upstream from the spectrometer. For clarity in the following discussion the start and stop times are defined in this way, although in practice an electronic clock or digitizer record would probably be started with the 'stop' time signal in order to increase the live time.

In addition to the time interval τ between start and stop, two other time intervals enter the problem. One is the time interval $\delta\tau$ for the electron to pass through the start detector, and the second is the time resolution $\Delta\tau$. We will assume for brevity that both of these are entirely associated with the start-time detection process.

The objective is to detect the electron without perturbing its motion to such an extent that its original energy can no longer be reliably measured in the spectrometer. An amount of energy ΔE must be extracted from the electron as it flies through the start detector in order to derive a trigger signal. The uncertainty in the start time is related to the uncertainty introduced in the electron's energy by

$$\Delta E \Delta\tau \geqslant \hbar. \tag{26}$$

Since $\hbar = 6.58 \times 10^{-7}$ eV ns, it is clear that the uncertainty principle is no impediment to a TOF measurement. This remains true even if one replaces $\Delta\tau$ by the much smaller quantity $\delta\tau$, arguing conservatively that the energy uncertainty should be related to the available observation time in the start detector, a time of order a few ns, instead of the desired TOF uncertainty, a time of order 100 ns.

Another, somewhat more stringent, criterion is that sufficient energy must be extracted from the electron to produce a signal that cannot be mistaken for a random fluctuation of thermal noise:

$$\Delta E \gg k_{\mathrm{B}} T. \tag{27}$$

Since $k_{\mathrm{B}} = 8.62 \times 10^{-5}\,\mathrm{eV\,K^{-1}}$, this condition presents no in-principle impediment to a TOF measurement either. On the other hand we do not want to change the energy of the tagged electron too much. Therefore equation (27) calls for a low-temperature detection device.

Notwithstanding these favourable indications, it is difficult to extract sufficient energy from a single electron moving in an apparatus of any size larger than microscopic. There are four methods that can be applied:

(i) radiation from an electron undergoing accelerated motion,
(ii) work done by image charges moving through a load circuit,
(iii) work done by magnetically induced currents flowing through a load circuit and
(iv) interaction of electrons with other electrons, e.g. in atoms.

We consider each of these approaches in turn.

5.1. Radiation from an electron undergoing accelerated motion

For low-energy or mildly relativistic electrons moving in a magnetic field, the dominant energy-loss mechanism is cyclotron radiation [40]. The power radiated scales as the square of the magnetic field B, and depends on the pitch angle θ with respect to the static field. The cyclotron angular frequency is

$$\omega = \frac{qB}{\gamma m_{\mathrm{e}}} \equiv \frac{\omega_0}{\gamma} \tag{28}$$

and the radiated power is

$$P(\beta, \theta) = \frac{1}{4\pi\epsilon_0} \frac{2q^2\omega_0^2}{3c} \frac{\beta^2 \sin^2\theta}{1-\beta^2}, \tag{29}$$

where q is the charge on the electron and m_{e} is the electron mass. At a field strength of 4.5 T, as is found between the KATRIN pre-spectrometer and the main spectrometer, the radiated power for 18.6 keV electrons having a 51° pitch angle is about 8 fW. If the observation region has a usable length x_m, the time spent by the electron in that region is

$$\delta\tau = \frac{x_m}{c\beta\cos\theta} \tag{30}$$

which, for $x_m = 50$ cm, ranges from 6 to 10 ns depending on the pitch angle. The energy lost by the electron in free radiation during its transit of the observation region is then $\leqslant 10^{-3}$ eV, only $12k_{\mathrm{B}}T$ at 1 K. The cyclotron frequency $\omega/2\pi$ is 126 GHz, still a technically challenging region to work in with non-bolometric amplifiers, and the antenna collection efficiency will necessarily be a compromise in order to allow the electrons to make an unobstructed transit.

More specifically, the noise power is $k_{\mathrm{B}}T\Delta\nu$, where $\Delta\nu$ is the bandwidth. There are two principal contributions to the bandwidth—the line broadening caused by the duration $\delta\tau$ of the signal, and the broadening caused by magnetic-field inhomogeneity. We assume the latter can be made smaller than the former, and neglect it. Only a fraction A of the radiated signal energy

is absorbed in the receiver. The signal power is distributed over a bandwidth $\Delta\nu = (2\pi\ \delta\tau)^{-1}$. Hence the energy from the signal W_s in the interval $\delta\tau$ may be compared with the noise energy W_n as follows:

$$W_s = AP(\beta, \theta)\delta\tau, \tag{31}$$

$$W_n = k_B T \Delta\nu\, \delta\tau, \tag{32}$$

$$\frac{W_s}{W_n} = \frac{2\pi AP(\beta, \theta)\delta\tau}{k_B T}. \tag{33}$$

Taking $\delta\tau = 10$ ns, the bandwidth is 16 MHz and the signal-to-noise ratio in that interval is about 16 when $\theta = 51^\circ$, $T = 1$ K and $A = 0.5$. The magnetic-field inhomogeneity must be less than about 10^{-4}. The signal-to-noise ratio drops rapidly below 51° pitch angle, which calls for a much longer magnet of high homogeneity.

Up to now we discussed classical electromagnetic radiation but we have to consider the quantization as well. The energy of a cyclotron radiation photon $E_{ph} = \hbar\omega$ amounts to 5×10^{-4} eV, which is comparable to the whole emitted radiation energy. This again calls for more radiated energy ΔE and thus for a longer magnetic field section.

5.2. Work done by image charges moving through a load circuit

Schottky pickups [36] encompass a broad class of devices used to detect particle beams without intercepting them. They have in common the induction of an image charge in a circuit connected to plates or a cavity. To estimate the energy that can be extracted from a single electron, we consider a conducting cylinder that the electron enters, passes through and emerges from. The image charge induced on the cylinder gives it a stored energy

$$W = \frac{q^2}{8\pi\epsilon_0 r}, \tag{34}$$

where r is the radius of the probe ring. For $r = 5$ cm, the stored energy is about 10^{-8} eV, which can be delivered to a suitably matched external circuit. Because the observation region x_m is considerably longer than the radius of the aperture, several probes can be cascaded to increase the energy extracted. If the probes are cascaded in a phased way, some further enhancement of the energy extraction can be achieved, but the dependence of electron transit times on pitch angle limits the usefulness of resonant structures.

5.3. Work done by magnetically induced currents flowing through a load circuit

The electron in flight produces a time-varying magnetic field that can be used to induce a transient current in a nearby inductively coupled element. The magnetic field can be obtained from a Lorentz transformation on a stationary electron

$$B(\zeta, t) = \frac{\mu_0}{4\pi} \frac{\gamma\beta cq\zeta}{(\zeta^2 + \gamma^2\beta^2c^2t^2)^{3/2}}, \tag{35}$$

where ζ is the impact parameter, or distance of closest approach, and t the time since closest approach. For the present purposes, we neglect the cyclotron motion because its period is two

orders of magnitude shorter than the characteristic time for establishing the magnetic field due to average linear motion. The magnetic energy in the field beyond a minimum radius $\zeta = r_i$ is

$$W = \pi \int_{r_i}^{\infty} \int_{-\infty}^{\infty} B^2 \beta \zeta c \, \mathrm{d}\zeta \, \mathrm{d}t \tag{36}$$

$$= \frac{3\pi^2}{4} \left(\frac{\mu_0}{4\pi}\right)^2 \frac{\gamma \beta^2 c^2 q^2}{r_i}. \tag{37}$$

The integral over time is equivalent to integrating over the third, axial, coordinate. Assuming all of the magnetic energy outside r_i can be delivered to an external circuit, the energy extracted from the electron is 1.6×10^{-15} eV for $r_i = 5$ cm. The estimate is somewhat pessimistic, because the spatial width of the instantaneous magnetic field distribution is considerably narrower than x_m, and so this amount of energy could be extracted several times with multiple inductors, but the available energy is so small that the details are not important.

5.4. Interaction of electrons with other electrons

This approach is standard and useful, but the energy extracted is not under control for any given collision, and sometimes may be much larger than desirable. Recently it has been proposed [37] to use highly excited Rydberg atoms as an interaction medium, since the cross section for modest energy losses is enhanced relative to more inelastic collisions.

5.5. Electron-tagger random triggers

In addition to the statistical advantage in measuring the signal, a substantial gain in background suppression can also be expected with electron tagging. The background suppression is based on the principle that a signal in the detector is placed in delayed coincidence with a signal from the tagger, within a time window of width t_o. Given a sufficiently low expected rate of tagger signals r_s, and neglecting pile-up, random coincidences would result in background reduction by a factor ϕ with

$$\frac{1}{\phi} = 1 - \mathrm{e}^{-t_o r_s}. \tag{38}$$

Too high a rate of tagger signals, either due to a high flux of incoming electrons or to a high noise level, would impair the measurement. However, in a dual-spectrometer setup like KATRIN, the electron flux through the tagger can be reduced by the pre-spectrometer down to $\mathcal{O}(10^3\ \mathrm{Hz})$. On the other hand, electrons can be trapped between the pre- and main spectrometer, and would give rise to a high rate of tagger signals. Trapped electrons, however, could be reduced by an active measure such as a scanning wire [38] or suitably chosen time-dependent perturbations of the electric fields along the transport path.

The tagger must be placed before the main spectrometer, but should be placed in a low rate area. For best tagger functionality, it is also favourable to have the beam tube through the tagger fill a small area. The highest-field region of the 4.5 T magnet between the pre-spectrometer and main spectrometer is a good position; there magnetic reflection reduces the flux through the

tagger even below the rate at the pre-spectrometer analysing plane. There are two major sources of electrons at this point in the beam line.

- Electrons from the source that make it through the pre-spectrometer, are reflected by the retarding potential at the main spectrometer analysing plane, and then go back through the pre-spectrometer and are absorbed in the source section. These will each pass the electron tagger twice.
- Electrons from the source that make it through the pre-spectrometer, are reflected by the main spectrometer, but, because of radiative losses or scattering inside the main spectrometer, lack the energy to make it back through the pre-spectrometer and become trapped. The rate of electrons becoming trapped is only $\mathcal{O}(1\,\mathrm{Hz})$, but, without any active removal method each trapped electron could pass the electron tagger millions of times before becoming undetectable. An active removal method only needs to remove trapped electrons in $\mathcal{O}(10^4$ passes) before the rate from trapped electrons is lower than the rate from electrons reflected by the main spectrometer retarding potential.

5.6. Random rate from pre-spectrometer

Electrons from the source that pass both the pre-spectrometer retarding potential, and the magnet, each make two passes.

From equation (5) applied to the pre-spectrometer, we find the magnet at the end of the pre-spectrometer reflects all electrons with a starting angle at the source greater than

$$\theta_{\mathrm{pre}} = \arcsin\left(\sqrt{\frac{B_{\mathrm{source}}}{B_{\mathrm{max}}}}\right), \tag{39}$$

where B_{max} is the magnetic field in the magnet at the end of the pre-spectrometer.

Solving equation (12) for E and requiring that the parallel momentum $p_{\|}$ must be positive to make it past the retarding potential, we find the minimum initial kinetic energy for passage through the pre-spectrometer is given by

$$E_{\mathrm{min}}(\theta, \Delta U, B) = \frac{\sqrt{kq^2\Delta U^2 + (k-1)^2 m_{\mathrm{e}}^2 c^4} + q\Delta U + (k-1)mc^2}{1-k}, \tag{40}$$

$$k = \sin^2\theta \frac{B(z_{\mathrm{pre}})}{B(z_{\mathrm{source}})},$$

where θ is the starting angle at the source, ΔU is the retarding potential of the pre-spectrometer and $B(z_{\mathrm{pre}})$ is the magnetic field at the analysing plane of the pre-spectrometer.

Combining equations (39) and (40) we find the average rate of electrons from the pre-spectrometer passing the electron tagger is

$$R_{\mathrm{pre}} = 2\int_0^{\theta_{\mathrm{pre}}} \frac{2\pi\ \sin\theta}{4\pi} \mathrm{d}\theta \int_{E_{\mathrm{min}}}^{E_0} \frac{\mathrm{d}N}{\mathrm{d}E}(\theta), \tag{41}$$

where $\frac{\mathrm{d}N}{\mathrm{d}E}(\theta)$ is the rate at the source, given by equation (20). The factor 2 has been applied since each electron makes two passes. This assumes that all electrons that make it through the pre-spectrometer are reflected by the main spectrometer, of which the vast majority are. The rate as a function of pre-spectrometer potential is plotted in figure 8. In figure 9 the neutrino mass sensitivity as a function of the rate at the tagger is plotted. It can be seen that rates below $\sim$10 kHz do not cause a significant loss of sensitivity.

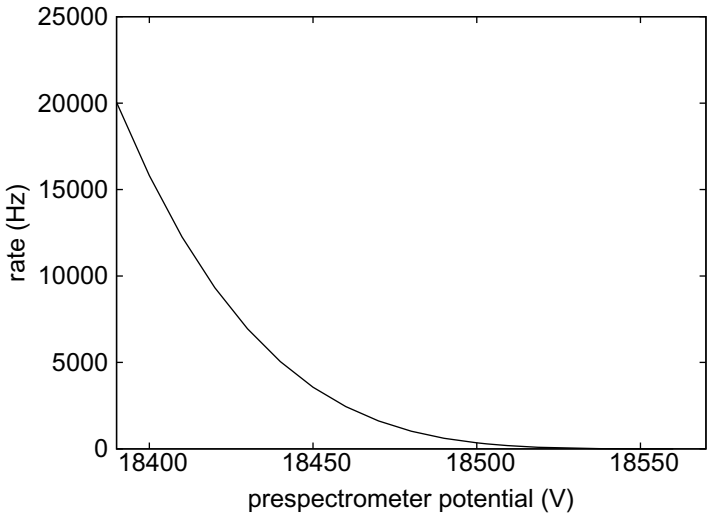

Figure 8. Rate of electrons passing the electron tagger, due to electrons which make it through the pre-spectrometer, are reflected in the main spectrometer, and return through the pre-spectrometer to be absorbed in the source section.

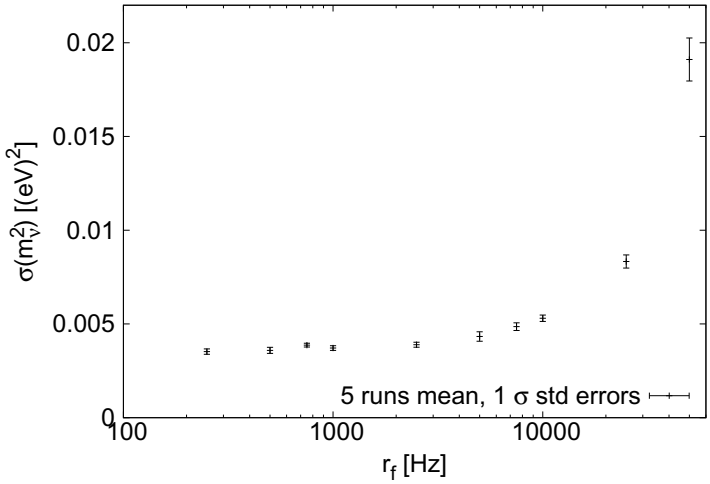

Figure 9. Statistical uncertainty of $m^2_{\nu_e}$ as a function of tagging rate r_f which is given by R_{pre} in equation (41), in case no other source of tagging events is present. The results are based on a measurement time distribution of 2/3 and 1/3 of three years in total, assigned to 18 565 and 18 560 eV, respectively (optimum distribution for 18 560 eV lowest retarding energy in table 1). For each point the results from five simulation runs with identical parameters and different random numbers have been averaged. Other sources of background and time resolution have been neglected.

5.7. Prospects for single-electron tagging

In summary, there is no fundamental obstacle to the detection of single electrons in flight, if the specification is only that energy perturbations be small enough to be acceptable for

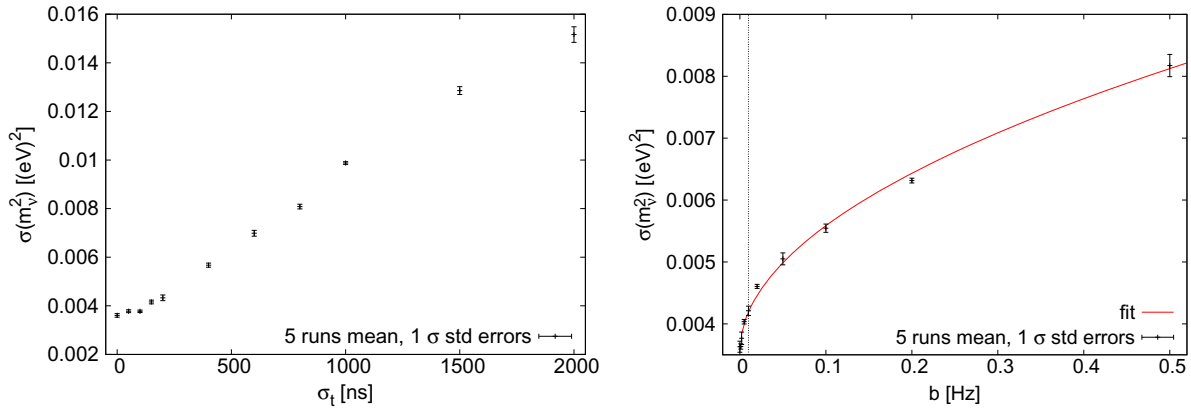

Figure 10. Statistical uncertainty of $m^2_{\nu_e}$ as a function of time resolution σ_t (a) and background rate b (b). The results are based on a measurement time distribution of 2/3 and 1/3 of 3 years in total, assigned to 18 565 and 18 560 eV, respectively (optimum distribution for 18 560 eV lowest retarding energy in table 1). In both plots the results from five simulation runs with identical parameters and different random numbers have been averaged. The dashed line in (b) corresponds to the KATRIN standard mode design goal of $b = 10$ mHz. The solid line in (b) represents the best fit by an inverse power law of the form $\sigma(x) = \sigma_0 + x^{1/a}$.

reliable energy determination. However, as a practical matter, no satisfactory method has yet been identified that allows a controlled and sufficiently large amount of energy to be extracted from the electron. The cyclotron-emission method may be adequately sensitive, but significantly longer superconducting magnets providing a very homogeneous field are needed at the tagger position, which are not available between the KATRIN spectrometers. With a successful tagger, there is the potential for suppression of backgrounds by virtue of the coincidence requirement between the electron tagger and the focal-plane detector, but there is also a random trigger rate for the tagger caused by electrons that do not pass through the main spectrometer.

6. Simulation of the measurement method

We turn now to numerical simulations in order to evaluate the performance of a TOF system under generic assumptions.

6.1. Generic parameters

Several parameters apply to most methods, chiefly the background rate, the time resolution and the efficiency. The dependence of the statistical uncertainty on the efficiency ϵ, i.e. the ratio of events whose TOF is correctly measured, follows a $1/\sqrt{\epsilon}$ law. This behaviour is theoretically predicted and has been verified by simulations. The dependence on the background rate and the time resolution found in the simulations is shown in figure 10.

For the time resolution a Gaussian uncertainty has been assumed. Figure 10 shows that the timing is uncritical for resolutions within the order of magnitude of the KATRIN detector. For resolutions in the range up to 200 ns the error increases by about 20%. The scale of this

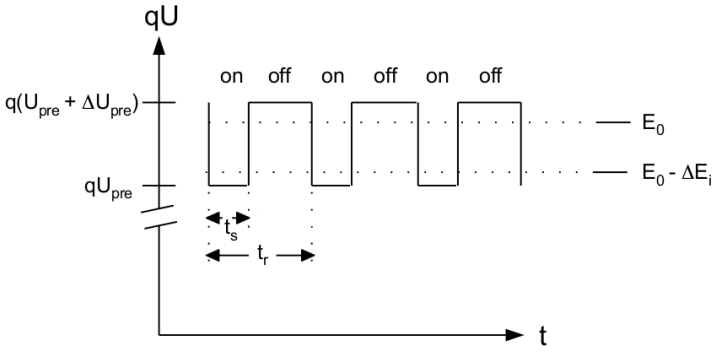

Figure 11. Timing parameters of the gated filter. X-axis: time. Y-axis: pre-spectrometer retarding potential. At the lower filter setting all electrons of the interesting region of width ΔE_i below the endpoint E_0 are transmitted while at the higher setting all electrons are blocked.

behaviour is plausible as the scale of the neutrino-mass-sensitive part of the TOF spectrum is mainly contained in the first few μs after the onset (see figure 6) and becomes washed out if the time resolution of the TOF measurement method exceeds some 100 ns.

Assuming the background level in the TOF mode is the same as in the standard mode where it is specified for KATRIN as $b < 10\,\mathrm{mHz}$, it can be shown that the improvement by the TOF mode is still up to a factor 3 in terms of $m^2_{\nu_\mathrm{e}}$. The behaviour follows a power law with approximately $\sigma_\mathrm{stat}(m^2_{\nu_\mathrm{e}}) = 0.006\,\mathrm{eV}^2/c^4 \times (b/\mathrm{Hz})^{1/2.0} + 0.004\,\mathrm{eV}^2/c^4$.[5] In comparison, in the standard mode the background dependence can be determined to be approximately $\sigma_\mathrm{stat}(m^2_{\nu_\mathrm{e}}) = 0.019\,\mathrm{eV}^2/c^4 \times (b/\mathrm{mHz})^{1/1.7} + 0.009\,\mathrm{eV}^2/c^4$ [39], in reasonable agreement with the analytically approximated formula of $\sigma_\mathrm{stat}(m^2_{\nu_\mathrm{e}}) \propto b^{1/3}$ [23].

6.2. *Gated filtering technique*

A method that has been discussed and successfully applied for TOF in the past is to periodically cut off the electron flux [41]. While there it has been used as a band-pass filter, where all signals with a TOF outside a certain time window have been rejected and a classic, non-integrated beta spectrum has been measured, this technique might as well be applied for TOF spectroscopy. In the case of KATRIN, periodic filtering could be achieved by a high-frequency modulation of the source or the pre-spectrometer potential.

The principle in this case is to switch between two settings. In one setting a pre-spectrometer potential $q(U_\mathrm{pre} + \Delta U_\mathrm{pre}) > E_0$ is chosen, to block completely the flux of β-electrons. In the other setting the retarding potential of the pre-spectrometer is set to $qU_\mathrm{pre} < E_0 - \Delta E_\mathrm{i}$, leading to the full transmission of all electrons from the interesting energy region $[E_0 - \Delta E_\mathrm{i}, E_0]$ and allowing to do TOF spectroscopy (see figure 11). The region of interest of width ΔE_i of a few 10 eV requires moderate switching voltages $\Delta U_\mathrm{pre} \approx -200\,\mathrm{V}$, taking into account the energy resolution of the pre-spectrometer of about 100 eV. While pulsing the source potential is the traditional approach as in [41], in a dual spectrometer set-up like KATRIN it thus is more convenient to vary the retarding potential of the pre-spectrometer. This has the

[5] Here, no correlation between background and starting signal as in the tagger case has been assumed.

advantage that, in contrast to pulsing at the source, the potential for the 'on'-setting does not need to be precise as long as a transmission of the region of interest is guaranteed.

6.2.1. Timing parameters. A periodically gated flux can in the simplest case be described by two timing parameters. The first one is the period t_r with which the flux is gated. After each period the detector clock is reset. The second one is the time t_s in which the gate is open in each period. The ratio of t_s and t_r gives the duty cycle

$$\eta = \frac{t_s}{t_r}. \tag{42}$$

This method uses no direct measurement of the starting times but restricts them to certain intervals of length t_s. That is equivalent to knowing the starting time with certain uncertainty. Thus, for $t_s \to 0$ and sufficient period lengths t_r, infinitesimally sharp starting times with infinitesimally low luminosity are obtained. If t_s is extended, the luminosity increases and the time uncertainty grows. The uncertainty is given by a uniform probability distribution in the interval $[0; t_s]$. As the measured TOF spectrum is then given by the convolution with the detection time and the starting time distribution,

$$\left(\frac{\mathrm{d}N}{\mathrm{d}t}\right)_{t_s} = \frac{\mathrm{d}N}{\mathrm{d}t} \otimes N(\sigma_\mathrm{d}) \otimes U(0, t_s), \tag{43}$$

where $N(\sigma_\mathrm{d})$ is the Gaussian uncertainty profile of the detection time at the detector and $U(0, t_s)$ is the uniform uncertainty due to the gate. If the detector clock is periodically reset with times t_r then some electrons with flight times $> t_r$ might hit the detector in a later period. Therefore, the final measured spectrum is a superposition of all contributing time distributions (43), shifted by multiples of t_r and finally cut off at 0 and t_r:

$$\left(\frac{\mathrm{d}N}{\mathrm{d}t}\right)_{t_s,t_r}(t) = \begin{cases} 0, & t < 0, \\ \sum_{n=0}^{\infty} \frac{\mathrm{d}N}{\mathrm{d}t}_{t_s}(t + n\,t_r), & 0 \leqslant t \leqslant t_r, \\ 0, & t > t_r. \end{cases}$$

As $> 99.5\%$ of the flight times lie within $\lesssim 50\,\mu$s,[6] all contributions with $nt_r \gtrsim t_s + 50\,\mu$s can be neglected. The resulting measured time spectrum (44) is strictly speaking not a spectrum of flight times, but rather of detection times for a periodically reset detector clock.

An illustrative TOF spectrum of simulated measurement data according to (44) is shown in figure 12. The two characteristics mentioned that describe a simple periodic gate show clear signatures in the curve. The uniform start time distribution within $[0, t_s]$ imposed on the spectrum by the uniform uncertainty (43) leads to a clear broadening of the shape. Since the time precision is lower than in the tagger case the broadening is more pronounced. In addition, the smearing with the step function leads to steeper edges than the Gaussian one. A clear sign of the detector resets are the residuals from former gate periods at the beginning of the spectrum. The effects of the timing parameters on the spectral shape allow some preliminary predictions on the effects of the performance:

- For constant t_s, reducing t_r will increase the duty cycle. However, more residuals from former periods contaminate the spectrum. That acts like a non-uniform background. Duty cycle and residual contributions need to be balanced.

[6] Under the condition that the retarding potential is at least some eV below the endpoint.

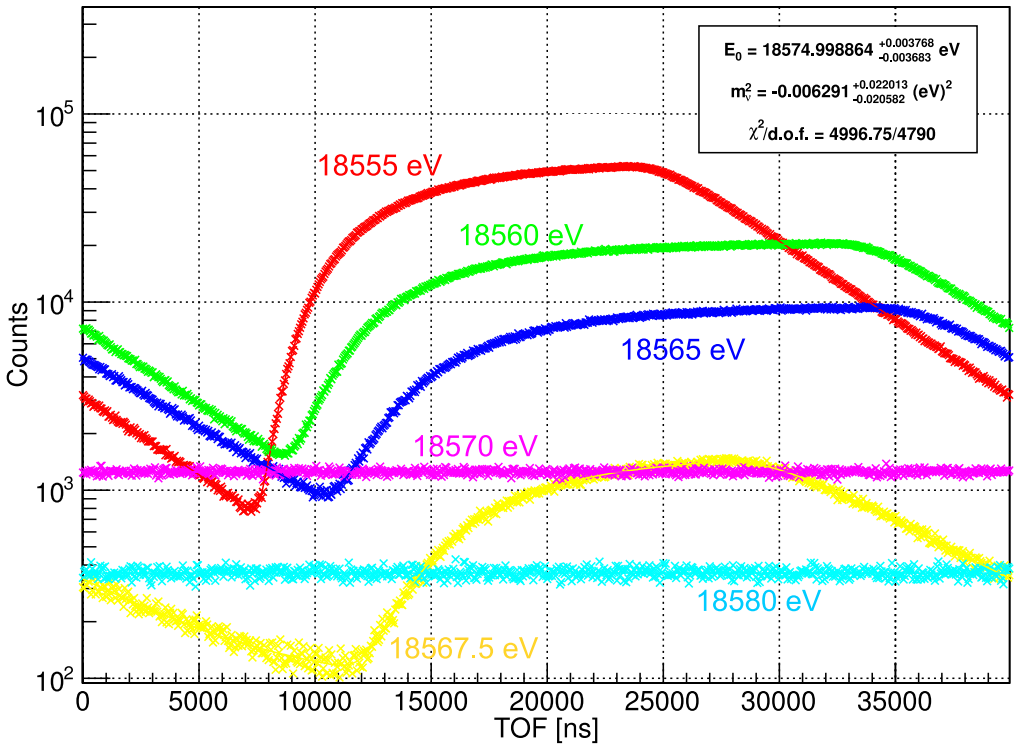

Figure 12. Example of simulated data of a TOF spectrum with a gated filter and fit. The colours correspond to the main spectrometer retarding energies. t_r is held constant at 40 μs while t_s and the measurement times per potential step have been chosen to match the optimal distribution stated in table 2. A total measurement time of three years has been assumed. On the left side of the spectrum the residuals from earlier cycles can be seen which emerge continuously from the end of the spectrum. The peaks exhibit effects of the convolution with the uniform start time distribution. For retarding energies of 18 570 and 18 570 eV the gated filter was always open ($t_s = t_r$) yielding time-independent count numbers. The other parameters in the simulation were $b_0 = 10^{-2}\,\mathrm{s}^{-1}$, $E_0 = 18\,575.0$ eV and $m^2_{\nu_e} = 0$.

- For constant t_r, reducing t_s will reduce the time uncertainty. In contrast, the duty cycle will be reduced, resulting in a lower count-rate. Here, the timing and the duty cycle need to be balanced.

Due to the trade-off between timing, duty cycle and residual background, the timing parameters need to be optimized. A global optimization of t_r and t_s has only shown a significant change in $\sigma_{\mathrm{stat}}(m^2_{\nu_e})$ for extreme input values. However, an individual optimization of t_s together with the measurement time contribution for each retarding energy makes sense, as for higher retarding potentials the count-rate drops while the neutrino mass information grows, so a higher duty cycle is needed. As the gated filter is less TOF-sensitive than an ideal TOF measurement, a higher number of retarding energies as well as measurements at lower retarding energies are necessary.

Table 2. Average statistical uncertainty $\langle\sigma_{\mathrm{stat}}(m^2_{\nu_e})\rangle = \langle\frac{1}{2}(|\Delta m^2_{\nu_e-}| + |\Delta m^2_{\nu_e+}|)\rangle$ (arithmetic mean of positive and negative error of ten simulations and fits), average fit parameters $\langle\bar{E}_0\rangle$ and $\langle\bar{m}^2_{\nu_e}\rangle$, as well as Pearson's correlation coefficient $R(E_0, m^2_{\nu_e})$ for uniform and optimized distribution of a gated filter setup. Assumed are 3 years measurement time with $m^2_{\nu_e} = 0\,\mathrm{eV}^2/c^4$, $E_0 = 18\,575.0\,\mathrm{eV}$ and $qU = 18\,555\,\mathrm{eV}$ as lowest retarding energy. The pulse period t_r was held constant at $40\,\mu\mathrm{s}$.

(Duty cycle t_s/t_r, measurement time fraction) at $qU =$						$\sigma_{\mathrm{stat}}(m^2_{\nu_e})$	$\langle\bar{E}_0\rangle$	$\langle\bar{m}^2_{\nu_e}\rangle$	$R(E_0, m^2_{\nu_e})$
18 555 V	18 560 V	18 565 V	18 567.5 V	18 570 V	18 575 V	(eV^2/c^4)	(eV^2/c^4)	(eV)	(eV^2/c^4)
$(0.5, \frac{1}{6})$	$(0.5, \frac{1}{6})$	$(0.5, \frac{1}{6})$	$(0.5, \frac{1}{6})$	$(0.5, \frac{1}{6})$	$(0.5, \frac{1}{6})$	0.025	18 574.9983	−0.0056	0.9230
$(0.4, \frac{1}{13})$	$(0.6, \frac{1}{13})$	$(0.6, \frac{2}{13})$	$(0.4, \frac{1}{13})$	$(1.0, \frac{4}{13})$	$(1.0, \frac{4}{13})$	0.021	18 575.0006	0.0049	0.8914

6.2.2. Results. The results of a rough optimization run with six retarding potentials, giving 12 free parameters, are shown in table 2. The highest retarding energy is above the endpoint that was assumed, thus being sensitive to the background level. Starting with $\eta = 0.5$ and a uniform distribution, each parameter has been scanned successively and set to the position of the local minimum. This has been repeated until the improvements per iteration are sufficiently small. The optimum has been found after five iterations. It can be seen that the optimization of duty cycles and measurement times provides an improvement of ∼30% compared to the uniform distribution with $\eta = 0.5$. The obtained result of $\sigma_{\mathrm{stat}}(m^2_{\nu_e}) = 0.021\,\mathrm{eV}^2/c^4$ is nearly identical with the standard KATRIN value of $\sigma_{\mathrm{stat}}(m^2_{\nu_e}) = 0.020\,\mathrm{eV}^2/c^4$ for the case of 20 eV difference between endpoint and lowest retarding energy. It remains open if a more detailed parameter optimization is able to increase the sensitivity.

7. Conclusion and outlook

A TOF spectroscopy mode could in principle provide significant improvements in the statistical neutrino mass sensitivity compared to a standard MAC-E-Filter mode. The study especially revealed the following information.

- In the standard mode it is necessary to measure at lower retarding potentials, for instance at KATRIN down to 30 eV below the endpoint, with a large number of measurement points.
- Using a TOF mode in contrast, it is sufficient to consider two or more retarding potentials only which may be even more close to the endpoint while improving the statistical uncertainty.
- This suggests that even the systematic uncertainty can be reduced with a TOF mode as the systematics grow with lower retarding potentials.

For a quantitative analysis of the improvement potential of the TOF mode relative to the standard mode one may consider figure 13, where the statistical uncertainty of $m^2_{\nu_e}$ is plotted as a function of the measurement interval below the endpoint E_0 (difference between lowest retarding potential and the endpoint E_0 using $E_0 = 18.575\,\mathrm{keV}$). Compared with the reference value of KATRIN, $\sigma_{\mathrm{stat}}(m^2_{\nu_e}) = 0.018\,\mathrm{eV}^2/c^4$ (see figure 13 curve (b) for measurement interval

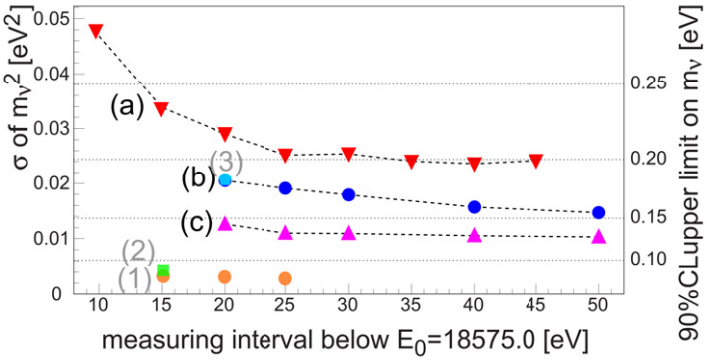

Figure 13. Statistical uncertainty $\sigma_{\mathrm{stat}}(m^2_{\nu_e})$ (3 years measurement time) and corresponding 90% CL upper limit on m_{ν_e} as a function of the analysed interval for different configurations of standard and TOF mode. Standard mode: (a) uniform measurement time; (b) optimized measurement time; (c) optimized measurement time, but background rate $b = 1$ mHz instead of 10 mHz as for (a) and (b). Results (a)–(c) and figure adapted from [18]. TOF spectroscopy (this work): (1) optimized measurement time, no background and infinite time resolution; (2) same as (1) for one exemplary measurement interval with a non-zero background rate $b = 10$ mHz; (3) gated filter with optimized measurement time and optimized duty cycle again for one exemplary measurement interval. Since it is well-known (e.g. [18]) that the systematic uncertainties increase with increasing measurement interval below the endpoint E_0 we have concentrated our TOF spectroscopy simulations to short measurement intervals, because otherwise any improvement in statistics might be overruled by systematic uncertainties.

of 30 eV), a statistical improvement of up to a factor 5 is possible in the optimal case (figure 13 (1)), equivalent to a factor of more than 2 in statistical sensitivity of m_{ν_e}. It can be shown (compare the difference in figure 13 between curves (b) and (c) w.r.t. point (2)) that this improvement factor is essentially not caused by neglecting the background but by intrinsic advantages of the method itself. A total improvement factor needs to take the systematics into account, which may only be simulated precisely if the measurement method is sufficiently known. This is especially true since both systematic and statistical uncertainty depend on the choice of retarding potentials, where an optimal trade-off has to be found.

Considering the measurement method, up to now no technique has been demonstrated that would allow a highly precise determination of the TOF of the electrons without disturbing their energy significantly. However, there is no fundamental obstacle to a measurement of this kind, and the main difficulty is one of extracting a sufficient and controlled amount of energy from the electron in flight. The most promising approach, nevertheless very challenging, is detection of the burst of cyclotron radiation as the electron passes through a zone of high magnetic field. If such a method existed, it would have the advantage of being not only a very sensitive implementation of the TOF mode, but also could significantly suppress backgrounds, depending on the total signal rate.

The method of a periodic gate, which has been tested in the context of the Mainz experiment [41], may be applied to TOF spectroscopy. The simulations, using a rough parameter

optimization, show that its sensitivity is comparable with the standard MAC-E mode (figure 13 point (3) and curve (b)). Hence, whether a TOF mode based on gated filtering is an improvement depends mainly on whether the systematics of that method are better or worse, compared with the standard method.

Apart from the measurement of the mass of the light active neutrinos, the gated filter may be of special interest for the detection of keV sterile neutrinos. In the WDM scenario, these additional neutrino mass states contribute to a large fraction of the dark matter in the universe and are weakly mixed with the electron neutrino [17]. As this mixing would give rise to a subtle 'kink' in the beta spectrum at $E_0 - m_4$, where $m_4 = \mathcal{O}(\text{keV})$ is the additional mass state, it might be useful to utilize a gated filter setup with narrow duty cycles providing sharp timing. The sharp gated filter reduces the statistics but a keV sterile ν signal will probably be limited by systematics in any case. There is the clear expectation that the TOF method will help in reducing the systematic uncertainty. The reason for this is that the TOF method as a differential method is able to disentangle the more energetic spectral parts, bearing no information about the sterile ν, from the sensitive parts near the potential barrier qU, within the region of the 'kink'. Thus, a significant part of the systematics, which would fully contribute in an integrating method, in which only the count-rate is measured, would have no effect on the sterile ν sensitivity.

For further investigation, a detailed study of systematics of a gated filter driven TOF mode is necessary. This could comprise experimental studies with an angular selective electron gun [42], theoretical considerations and MC simulations. It may also be useful to investigate the statistics of the gated filter in more detail, considering more parameters to be optimized.

Acknowledgments

This work was partly supported by BMBF under contract number 05A11PM2 and by the US Department of Energy under grant DE-FG02-97ER41020.

References

[1] Kim S B, Lasserre T and Wang Y 2013 Reactor neutrinos *Adv. High Energy Phys.* **2013** 453816
[2] Antonelli V, Miramonti L, Pena Garay C and Serenelli A 2013 Solar neutrinos *Adv. High Energy Phys.* **2013** 351926
[3] Kajita T 2012 Atmospheric neutrinos *Adv. High Energy Phys.* **2012** 504715
[4] Feldman G J, Hartnell J and Kobayashi T 2013 Long-baseline neutrino oscillation experiments *Adv. High Energy Phys.* **2013** 475749
[5] Dore U and Orestano D 2008 Experimental results on neutrino oscillations *Rep. Prog. Phys.* **71** 106201
[6] Ade P A R *et al* (Planck Collaboration) 2013 Planck results XVI: cosmological parameters *Astron. Astrophys.* submitted (arXiv:1303.5076 [astro-ph.CO])
[7] Giunti C and Kim C W 2007 *Fundamentals of Neutrino Physics and Astrophysics* (Oxford: Oxford University Press)
[8] Mention G *et al* 2011 Reactor antineutrino anomaly *Phys. Rev.* D **83** 073006
[9] Anselmann P *et al* 1995 GALLEX solar neutrino observations: complete results for GALLEX II *Phys. Lett.* B **357** 237–47
[10] Kaether F *et al* 2010 Reanalysis of the Gallex solar neutrino flux and source experiments *Phys. Lett.* B **685** 47
[11] Abdurashitov J N *et al* 2006 Measurement of the response of a Ga solar neutrino experiment to neutrinos from a ^{37}Ar source *Phys. Rev.* C **73** 045805

[12] Abdurashitov J N *et al* 2009 Measurement of the solar neutrino capture rate with gallium metal: III. Results for the 2002–2007 data-taking period *Phys. Rev.* C **80** 015807
[13] Athanassopoulos C *et al* 1998 Results on $\nu_\mu \rightarrow \nu_e$ neutrino oscillations from the LSND experiment *Phys. Rev. Lett.* **81** 1774
[14] Aguilar-Arevalo A A *et al* 2007 Search for electron neutrino appearance at the $\Delta m^2 \approx 1\,\mathrm{eV}^2$ scale *Phys. Rev. Lett.* **98** 231801
[15] Steigman G 2012 Neutrinos and big bang nucleosynthesis *Adv. High Energy Phys.* **2012** 268321
[16] Valentino E D *et al* 2013 Tickling the CMB damping tail: scrutinizing the tension between the ACT and SPT experiments arXiv:1301.7343
[17] Biermann P L, de Vega H J and Sanchez N G 2013 Towards the Chalonge Meudon workshop 2013. Highlights and conclusions of the Chalonge Meudon workshop 2012: warm dark matter galaxy formation in agreement with observations arXiv:1305.7452
[18] Angrik J *et al* (KATRIN Collaboration) *KATRIN Design Report 2004* Wissenschaftliche Berichte, FZ Karlsruhe 7090 (http://bibliothek.fzk.de/zb/berichte/FZKA7090.pdf)
[19] Drexlin G, Hannen V, Mertens S and Weinheimer C 2013 Current direct neutrino mass experiments *Adv. High Energy Phys.* **2013** 293986
[20] Kraus Ch *et al* 2005 Final results from phase II of the Mainz neutrino mass search in tritium beta decay *Eur. Phys. J.* C **40** 447–68
[21] Aseev V N *et al* 2011 Upper limit on the electron antineutrino mass from the Troitsk experiment *Phys. Rev.* D **84** 112003
[22] Giuliani A and Poves A 2012 Neutrinoless double-beta decay *Adv. High Energy Phys.* **2012** 857016
[23] Otten E W and Weinheimer C 2008 Neutrino mass limit from tritium β decay *Rep. Prog. Phys.* **71** 086201
[24] Saenz A, Jonsell S and Froelich P 2000 Improved molecular final-state distribution of HeT^+ for the β-decay process of T_2 *Phys. Rev. Lett.* **84** 242–5
[25] Doss N, Tennyson J, Saenz A and Jonsell S 2006 Molecular effects in investigations of tritium molecule β decay endpoint experiments *Phys. Rev.* C **73** 025502
[26] Doss N and Tennyson J 2008 Excitations to the electronic continuum of $^3HeT^+$ in investigations of T_2 β-decay experiments *J. Phys. B: At. Mol. Opt. Phys.* **41** 125701
[27] Picard A *et al* 1992 A solenoid retarding spectrometer with high resolution and transmission for keV electrons *Nucl. Instrum. Methods* B **63** 345–58
[28] Aseev V N *et al* 2000 Energy loss of 18 keV electrons in gaseous T_2 and quench condensed D_2 films *Eur. Phys. J.* D **10** 39–52
[29] Nagy Sz *et al* 2006 On the Q-value of the tritium β-decay *Europhys. Lett.* **74** 404
[30] Blaum K, Novikov Yu N and Werth G 2010 Penning traps as a versatile tool for precise experiments in fundamental physics *Contemp. Phys.* **51** 149–75
[31] Babutzka M *et al* 2012 Monitoring of the operating parameters of the KATRIN windowless gaseous tritium source *New J. Phys.* **14** 103046
[32] Cowan G 1998 *Statistical Data Analysis (Oxford Science Publications)* (Oxford: Oxford University Press)
[33] Valerius K 2009 Spectrometer-related background processes and their suppression in the KATRIN experiment *PhD Thesis* Westfälische Wilhelms-Universität Münster
[34] Glück F to be published
[35] Weinheimer Ch *et al* 1993 Improved limit on the electron-antineutrino rest mass from tritium β-decay *Phys. Lett.* B **300** 210–6
[36] Franzke B *et al* 1995 Schottky mass spectrometry at the experimental storage ring ESR *Phys. Scr.* **1995** 176
[37] Jerkins M, Klein J R, Majors J H, Robicheaux F and Raizen M G 2010 Using cold atoms to measure neutrino mass *New J. Phys.* **12** 043022
[38] Beck M *et al* 2010 Effect of a sweeping conductive wire on electrons stored in a Penning-like trap between the KATRIN spectrometers *Eur. Phys. J.* A **44** 499–511
[39] Mertens S *et al* 2013 Background due to stored electrons following nuclear decays in the KATRIN spectrometers and its impact on the neutrino mass sensitivity *Astropart. Phys.* **41** 52–62

[40] Monreal B and Formaggio J A 2009 Relativistic cyclotron radiation detection of tritium decay electrons as a new technique for measuring the neutrino mass *Phys. Rev.* D **80** 051301

[41] Bonn J, Bornschein L, Degen B, Otten E W and Weinheimer Ch 1999 A high resolution electrostatic time-of-flight spectrometer with adiabatic magnetic collimation *Nucl. Instrum. Methods* A **421** 256

[42] Valerius K, Beck M, Arlinghaus H, Bonn J, Hannen V M, Hein H, Ostrick B, Streubel S, Weinheimer Ch and Zbořil M 2009 A UV led-based fast-pulsed photoelectron source for time-of-flight studies *New J. Phys.* **11** 063018